

# Photoelectron spectra in an autoionization system interacting with a neighboring atom

Jan Peřina Jr.,<sup>1</sup> Antonín Lukš,<sup>2</sup> Wiesław Leoński,<sup>3</sup> and Vlasta Peřinová<sup>2</sup>

<sup>1</sup>*Institute of Physics of AS CR, Joint Laboratory of Optics,  
17. listopadu 50a, 772 07 Olomouc, Czech Republic*

<sup>2</sup>*Palacký University, RCPTM, Joint Laboratory of Optics,  
17. listopadu 12, 771 46 Olomouc, Czech Republic*

<sup>3</sup>*Quantum Optics and Engineering Division, Institute of Physics,  
University of Zielona Góra, Prof. Z. Szafrana 4a, 65-516 Zielona Góra, Poland*

Photoelectron ionization spectra of an autoionization system with one discrete level interacting with a neighbor two-level atom are discussed. The formula for long-time ionization spectra is derived. According to this formula, the spectra can be composed of up to eight peaks. Moreover, the Fano-like zeros for weak optical pumping have been identified in these spectra. The conditional ionization spectra depending on the state of the neighbor atom exhibit oscillations at the Rabi frequency. Dynamical spectral zeros occurring once per the Rabi period have been revealed in these spectra.

PACS numbers: 32.80.-t, 33.80.Eh, 34.20.-b

## I. INTRODUCTION

The problem of ionization of an atom with discrete autoionizing levels has been addressed many times under various conditions since the pioneering work by Fano [1] appeared. In his contribution, Fano has explained the existence of unpopulated frequencies in the continuum of ionized states by diagonalizing the appropriate Hamiltonian. This effect occurs as a consequence of destructive interference of two quantum ionization paths. This phenomenon occurring at specific frequencies (or for given ionization states) is spoken of as the presence of 'Fano zeros'. Moreover, there might occur a strong narrowing of spectral peaks in the vicinity of such frequencies by virtue of strong interference. This effect is sometimes referred to as the 'confluence of bound-free coherences' [2]. These effects can be degraded to certain extent by, e.g., spontaneous emission of radiation [3–5], finite pump laser bandwidth [6] or collisions [5]. In general, there exist  $n$  Fano zeros in an autoionization system with  $n$  discrete autoionizing levels [1, 7]. Generalizations including several mutually non-interacting continua has also been given [1, 8]. The presence of autoionizing levels also influences ionization dynamics under strong laser pumping [9]. Experimental observation of Fano spectral zeros has been reported, e.g., in [10]. The existence of discrete levels in autoionization systems can lead to transparency for ultra-short pulses [11] or slowing-down of propagating light [12]. The dynamics of ionization can be even influenced by the Zeno or anti-Zeno effects [13]. A generalization to low-light quantum optical fields including the Fock coherent or squeezed states has also been given [14, 15] and it has revealed additional interferences in photoelectron ionization spectra stemming from the discrete energies of quantized optical fields. The studied ionization quantum-path interference effects play an important role in spectroscopy in explaining asymmetric spectral profiles [16]. Similar quantum interference ef-

fects can be found in many other fields of physics, both using mass particles and photons. Among others, semiconductor hetero-structures or photonic waveguides can be mentioned [17]. An extended list of references dealing with autoionization can be found in [5, 7, 18].

In this work we continue the investigation of the influence of a neighbor atom to an ionization system and its long-time photoelectron ionization spectra. The influence is assumed to have the form of energy transfer caused, e.g., by the dipole-dipole interaction. Compared to [19], we additionally assume one discrete bound (autoionizing) state present in the ionization system. Similarly as in [19], the neighbor atom is modelled as a two-level system that undergoes Rabi oscillations in a stationary optical field. These oscillations significantly influence conditional photoelectron spectra of the autoionization system. In these spectra, the so-called dynamical zeros occurring once per the Rabi period [19] have been found. Frequencies in photoelectron ionization spectra corresponding to both the Fano-like zeros (for weak optical pumping) and the dynamical zeros are studied using both analytical and numerical approaches. Molecular condensates [20] as well as systems of quantum dots or other semiconductor hetero-structures [17] are suitable candidates for the verification of the obtained results.

The paper is organized as follows. Sec. II brings the model Hamiltonian, solution of the corresponding Schrödinger equation and formulas for photoelectron ionization spectra. These spectra in their long-time limit are discussed in Sec. III. The frequencies of Fano-like zeros in the spectra are analyzed in Sec. IV using the method of canonical transformation. Sec. V is devoted to dynamical zeros. Conclusions are drawn in Sec. VI. Formulas giving the frequencies of poles of the Lorentzian curves constituting the photoelectron ionization spectra can be found in Appendix A. A method for the determination of frequencies of the Fano as well as dynamical zeros is developed in Appendix B.

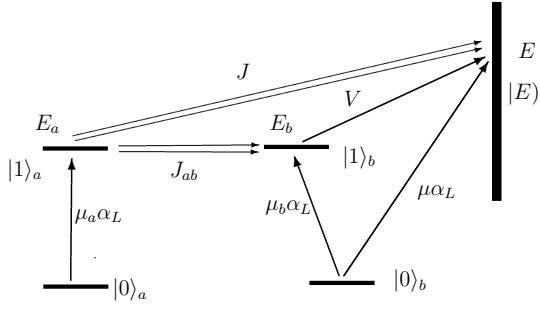


FIG. 1. Scheme of the autoionization system  $b$  interacting with a two-level atom  $a$ . State  $|1\rangle_a$  means an excited state of atom  $a$  with the energy  $E_a$ ,  $|1\rangle_b$  stands for an excited bound state of autoionization system  $b$  with the energy  $E_b$ , and  $|E\rangle$  is a free state inside the continuum at the atom  $b$  with the energy  $E$ . Symbols  $\mu_a$ ,  $\mu_b$ , and  $\mu$  denote the dipole moments between the ground states  $|0\rangle_a$  and  $|0\rangle_b$  and the corresponding excited states,  $\alpha_L$  stands for the pumping amplitude,  $V$  describes the Coulomb configurational coupling between the states  $|1\rangle_b$  and  $|E\rangle$ , and  $J$  [ $J_{ab}$ ] refers to the dipole-dipole interaction between the states  $|1\rangle_a$  and  $|E\rangle$  [ $|1\rangle_b$ ]. Double arrows indicate that two electrons at the atoms  $a$  and  $b$  participate in the interaction (energy transfer).

## II. QUANTUM MODEL AND ITS PHOTOELECTRON IONIZATION SPECTRA

The considered ionization system (atom, molecule) with one autoionizing level is assumed to interact with a neighbor two-level atom (molecule) by the dipole-dipole interaction (for the scheme, see Fig. 1). Both the ionization system and the neighbor atom are under the influence of a stationary optical field. The Hamiltonian  $\hat{H}_{a-i}$  of the ionization system  $b$  with one autoionizing level can be written in the form ( $\hbar = 1$  is assumed, [21]):

$$\begin{aligned} \hat{H}_{a-i} = & E_b |1\rangle_b \langle 1| + \int dE E |E\rangle \langle E| \\ & + \int dE (V |E\rangle_b \langle 1| + \text{H.c.}) \\ & + [\mu_b \alpha_L \exp(-iE_L t) |1\rangle_b \langle 0| + \text{H.c.}] \\ & + \int dE [\mu \alpha_L \exp(-iE_L t) |E\rangle_b \langle 0| + \text{H.c.}]. \end{aligned} \quad (1)$$

In Eq. (1), the symbol  $E_b$  means the excitation energy from the ground state  $|0\rangle_b$  into the excited bound state  $|1\rangle_b$  of atom  $b$ . The continuum of the autoionization system  $b$  is formed by the states  $|E\rangle$  with their energies  $E$ . The coupling constant  $V$  describes the Coulomb configuration interaction between the states  $|1\rangle_b$  and  $|E\rangle$  inside the continuum. The dipole moments  $\mu_b$  and  $\mu$  characterize the optical excitation of the corresponding states;  $\alpha_L$  means an optical-field amplitude oscillating at the frequency  $E_L$ . The symbol H.c. stands for the Hermitian conjugated term.

A neighbor two-level atom  $a$  interacting with the optical field through the dipole moment  $\mu_a$  is described by

the Jaynes-Cummings Hamiltonian  $\hat{H}_{t-a}$ :

$$\hat{H}_{t-a} = E_a |1\rangle_a \langle 1| + [\mu_a \alpha_L \exp(-iE_L t) |1\rangle_a \langle 0| + \text{H.c.}]. \quad (2)$$

The energy  $E_a$  of the excited bound state  $|1\rangle_a$  of the atom  $a$  is measured relative to the energy of the ground state  $|0\rangle_a$ . The ground states of atoms  $a$  and  $b$  are assumed to have the same energy that is chosen to be zero.

The energy transfer [20] caused by the dipole-dipole interaction between the two-level atom  $a$  and the autoionizing system  $b$  is characterized by the Hamiltonian  $\hat{H}_{\text{trans}}^e$ :

$$\begin{aligned} \hat{H}_{\text{trans}}^e = & [J_{ab} |1\rangle_b \langle 0| |0\rangle_a \langle 1| + \text{H.c.}] \\ & + \int dE [J |E\rangle_b \langle 0| |0\rangle_a \langle 1| + \text{H.c.}]. \end{aligned} \quad (3)$$

In this interaction, one electron loses its energy when returning from the excited state into the ground state, whereas the other one absorbs this energy and moves from the ground state into its own excited state. The constants  $J_{ab}$  and  $J$  quantify the strength of this interaction.

A general quantum state of two electrons at the atoms  $a$  and  $b$  can be written in the following form appropriate to the rotating frame:

$$\begin{aligned} |\psi\rangle(t) = & c_{00}(t) |0\rangle_a |0\rangle_b + c_{10}(t) |1\rangle_a |0\rangle_b \\ & + c_{01}(t) |0\rangle_a |1\rangle_b + c_{11}(t) |1\rangle_a |1\rangle_b \\ & + \int dE d_0(E, t) |0\rangle_a |E\rangle \\ & + \int dE d_1(E, t) |1\rangle_a |E\rangle. \end{aligned} \quad (4)$$

The time-dependent coefficients  $c_{00}$ ,  $c_{10}$ ,  $c_{01}$ ,  $c_{11}$ ,  $d_0(E)$ , and  $d_1(E)$  characterize the state  $|\psi\rangle$  at an arbitrary time.

The Schrödinger equation with the Hamiltonian  $\hat{H}_{a-i} + \hat{H}_{t-a} + \hat{H}_{\text{trans}}^e$  can be written as a system of differential equations for the coefficients of decomposition written in Eq. (4):

$$i \frac{d}{dt} \begin{bmatrix} \mathbf{c}^e(t) \\ \mathbf{d}(E, t) \end{bmatrix} = \begin{bmatrix} \mathbf{A}^e & \mathbf{B}^e \int dE \\ \mathbf{B}^{e\dagger} & \mathbf{K}(E) \end{bmatrix} \begin{bmatrix} \mathbf{c}^e(t) \\ \mathbf{d}(E, t) \end{bmatrix}. \quad (5)$$

The symbol  $\dagger$  denotes the Hermitian conjugation. The vectors  $\mathbf{c}^e$  and  $\mathbf{d}$  and the matrices  $\mathbf{A}^e$ ,  $\mathbf{B}^e$ , and  $\mathbf{K}$  introduced in Eq. (5) can be derived in the form:

$$\begin{aligned} \mathbf{c}^e(t) = & \begin{bmatrix} c_{00}(t) \\ c_{10}(t) \\ c_{01}(t) \\ c_{11}(t) \end{bmatrix}, \quad \mathbf{d}(E, t) = \begin{bmatrix} d_0(E, t) \\ d_1(E, t) \end{bmatrix}, \quad (6) \\ \mathbf{A}^e = & \begin{bmatrix} 0 & \mu_a^* \alpha_L^* & \mu_b^* \alpha_L^* & 0 \\ \mu_a \alpha_L & \Delta E_a & J_{ab}^* & \mu_b^* \alpha_L^* \\ \mu_b \alpha_L & J_{ab} & \Delta E_b & \mu_a^* \alpha_L^* \\ 0 & \mu_b \alpha_L & \mu_a \alpha_L & \Delta E_a + \Delta E_b \end{bmatrix}, \end{aligned} \quad (7)$$

$$\mathbf{B}^e = \begin{bmatrix} \mu^* \alpha_L^* & 0 \\ J^* & \mu^* \alpha_L^* \\ V^* & 0 \\ 0 & V^* \end{bmatrix}, \quad (8)$$

$$\mathbf{K}(E) = \begin{bmatrix} E - E_L & \mu_a^* \alpha_L^* \\ \mu_a \alpha_L & E - E_L + \Delta E_a \end{bmatrix}; \quad (9)$$

$\Delta E_a = E_a - E_L$  and  $\Delta E_b = E_b - E_L$ . As the electrons remain inside the system during the evolution, the norm of state  $|\psi\rangle$  is preserved:

$$\sum_{j,k=0}^1 |c_{jk}(t)|^2 + \sum_{j=0}^1 \int dE |d_j(E, t)|^2 = 1. \quad (10)$$

The system of differential equations (5) can be solved using the Laplace-transform method (for details, see [19]). The coefficients  $d_0(E, t)$  and  $d_1(E, t)$  of the solution then give the amplitude photoelectron ionization spectra of atom  $b$  conditioned by the presence of atom  $a$  in the ground and excited states, respectively. It can be shown that, in the solution, there exist two prominent frequencies  $\xi_1$  and  $\xi_2$  characterizing oscillations of the neighbor atom  $a$ ;

$$\xi_{1,2} = E_L - \frac{\Delta E_a \pm \delta\xi}{2}, \quad (11)$$

$$\delta\xi = \sqrt{(\Delta E_a)^2 + 4|\mu_a \alpha_L|^2}.$$

The solution for the coefficients  $\mathbf{d}(E, t)$  can be derived as follows [19]:

$$\mathbf{d}(E, t) = \mathbf{d}^{\xi_1}(E, t) + \mathbf{d}^{\xi_2}(E, t), \quad (12)$$

$$\mathbf{d}^{\xi_j}(E, t) = i\mathbf{K}_j \mathbf{B}^{e\dagger} \mathbf{P}^e \mathbf{U}_k^e(E, t) \mathbf{P}^{e-1} \mathbf{c}^e(0), \quad (13)$$

$$j = 1, 2.$$

The elements of the diagonal evolution matrices  $\mathbf{U}_k^e$ ,  $k = 1, 2$ , in Eq. (13) are given as:

$$[\mathbf{U}_k^e]_{jl}(E, t) = \frac{i\delta_{jl}}{E - \Lambda_{M^{e,j}} - \xi_k} [\exp[i(\xi_k - E)t] - \exp(-i\Lambda_{M^{e,j}}t)]; \quad (14)$$

$\delta_{jk}$  being the Kronecker symbol. The symbols  $\Lambda_{M^{e,j}}$  denote eigenvalues of the evolution matrix  $\mathbf{M}^e$ ,  $\mathbf{M}^e = \mathbf{A}^e - i\pi \mathbf{B}^e \mathbf{B}^{e\dagger}$ . The eigenvectors of matrix  $\mathbf{M}^e$  then form the columns of matrix  $\mathbf{P}^e$  introduced in Eq. (13). The matrices  $\mathbf{K}_k$  occurring in Eq. (13) take the form:

$$\mathbf{K}_k = \frac{(-1)^k}{\delta\xi} \begin{bmatrix} E_a + \xi_k & -\mu_a^* \alpha_L^* \\ -\mu_a \alpha_L & E_L + \xi_k \end{bmatrix}. \quad (15)$$

The vector  $\mathbf{c}^e(0)$  in Eq. (13) gives the initial conditions. We assume here that electrons at both the two-level atom  $a$  and the autoionizing system  $b$  are initially in their ground states, i.e.  $\mathbf{c}^e(0) = (1, 0, 0, 0)$ .

In deriving the long-time photoelectron ionization spectra, the long-time form of the evolution matrices  $\mathbf{U}_k^e$  defined in Eq. (14) is needed:

$$[\mathbf{U}_k^{e, \text{lt}}]_{jl}(E, t) = \frac{i\delta_{jl} \exp[i(\xi_k - E)t]}{E - \Lambda_{M^{e,j}} - \xi_k}. \quad (16)$$

We note that the formula in (16) is valid for the times  $t$  obeying  $t \gg 1/|\text{Im}\{\Lambda_{M^{e,j}}\}|$  for  $j = 1, \dots, 4$ ; the symbol  $\text{Im}$  means the imaginary part. The long-time form of evolution matrices  $\mathbf{U}_1^{e, \text{lt}}$  and  $\mathbf{U}_2^{e, \text{lt}}$  shows that oscillations at the Rabi frequency  $\delta\xi = \xi_1 - \xi_2$  occur in the intensity photoelectron ionization spectra  $I_j^{\text{lt}}$ ,  $I_j^{\text{lt}}(E) \equiv |d_j^{\text{lt}}|^2(E)$ . A detailed analysis has shown [19] that the long-time intensity spectra  $I_0^{\text{lt}}$  and  $I_1^{\text{lt}}$  can be expressed in a specific form:

$$I_0^{\text{lt}}(E, t) = I_0^{\text{st}}(E) + I^{\text{osc}}(E) \cos[\delta\xi t + \varphi(E)],$$

$$I_1^{\text{lt}}(E, t) = I_1^{\text{st}}(E) - I^{\text{osc}}(E) \cos[\delta\xi t + \varphi(E)]. \quad (17)$$

The intensities  $I_0^{\text{st}}$  and  $I_1^{\text{st}}$  denote the steady-state parts of the corresponding spectra, whereas the intensity  $I^{\text{osc}}$  describes the magnitude of harmonic oscillations between the spectra  $I_0^{\text{lt}}$  and  $I_1^{\text{lt}}$ . The symbol  $\varphi$  stands for a spectrally dependent phase. These temporal oscillations at the Rabi frequency in the conditional long-time photoelectron ionization spectra can be observed using the time-resolved spectroscopy of photo-ionized electrons [21]. If the temporal resolution is not sufficient, only the steady-state parts  $I_0^{\text{st}}(E)$  and  $I_1^{\text{st}}(E)$  are experimentally available. We note that the Rabi oscillations can alternatively be observed in the long-time behavior of the two-level atom  $a$  provided that a suitable basis in the continuum of ionized states of atom  $b$  is chosen and a conditional measurement into its basis functions is considered.

The form of long-time spectra  $I_0^{\text{lt}}$  and  $I_1^{\text{lt}}$  as written in Eq. (17) guarantees that the overall long-time photoelectron ionization spectrum  $I^{\text{lt}}(E) = I_0^{\text{lt}}(E, t) + I_1^{\text{lt}}(E, t)$  is time independent;

$$I^{\text{lt}}(E) = I_0^{\text{st}}(E) + I_1^{\text{st}}(E). \quad (18)$$

In the long-time photoelectron ionization spectra, there may occur frequencies that cannot be populated. If a given frequency  $E_F$  cannot be excited for arbitrary times, we have a Fano zero obeying the following equation:

$$I^{\text{lt}}(E_F) = 0. \quad (19)$$

According to Eq. (18) a Fano zero at the frequency  $E_F$  is present only if  $I_0^{\text{st}}(E_F) = 0$  and  $I_1^{\text{st}}(E_F) = 0$ .

It may also happen that the long-time spectral components  $I_0^{\text{st}}$ ,  $I_1^{\text{st}}$ , and  $I^{\text{osc}}$  fulfil one or both of the following equations for specific frequencies  $E_D$ :

$$I_j^{\text{st}}(E_D) = I^{\text{osc}}(E_D), \quad j = 0, 1. \quad (20)$$

This means that the long-time photoelectron ionization spectrum  $I_0^{\text{lt}}(E, t_D)$  [or  $I_1^{\text{lt}}(E, t_D)$ ] reaches zero at suitable time instants  $t_D$ . Such a frequency  $E_D$  corresponds to a dynamical zero that periodically occurs with the Rabi period  $2\pi/\delta\xi$  [19]. We note that dynamical zeros occur, because of the interaction of the autoionization system  $b$  with the two-level atom  $a$ . The frequencies of

dynamical zeros depend, in general, on the state of the two-level atom  $a$ . However, if the two-level atom  $a$  is resonantly pumped, these frequencies in the long-time photoelectron spectra  $I_0^{\text{lt}}$  and  $I_1^{\text{lt}}$  coincide. We note that a Fano zero also obeys the conditions in Eq. (20) defining a dynamical zero.

### III. PHOTOELECTRON IONIZATION SPECTRA

The long-time photoelectron ionization spectra of the Fano model as well as the ionization system interacting with a neighbor atom studied in [19] are useful in the analysis of the spectra belonging to the autoionization system interacting with a neighbor. That is why, we refer to them in the discussion below.

The general form of amplitude photoelectron ionization spectra  $\mathbf{d}(E, t)$  of the interacting autoionization system is composed of eight Lorentzian curves as the formulas in Eqs. (12), (13), and (16) show. These curves are located at different frequencies  $E_r$  in the complex plane  $E$ . The complex frequencies  $E_r$  differ in magnitudes of their complex parts and so they lead to peaks of different widths on the real axis  $E$ . In more detail, there exist two groups of four of the frequencies  $E_r$  (see Appendix A). The frequencies  $E_r$  from the second group are just those of the first group shifted by the Rabi frequency  $\delta\xi$ . However, as numerical results have revealed, only four frequencies  $E_r$  (two pairs) are important for the determination of shapes of the photoelectron ionization spectra  $I^{\text{lt}}$  in two regimes discussed here and assuming resonant pumping of atom  $a$ .

In order to demonstrate the main features found in the photoelectron ionization spectra, we first consider the comparable 'ionization' interactions at atoms  $a$  and  $b$  ( $V \approx J, J_{ab}$ ). The regime with  $V \gg J, J_{ab}$  appropriate for molecular condensates is analyzed subsequently.

Analyzing the long-time photoelectron ionization spectra, we first consider a weak direct ionization ( $q_a, q_b \gg 1$ , for the definition of parameters, see the caption to Fig. 2). On assuming equally strong indirect ionization paths through the states  $|1\rangle_a$  and  $|1\rangle_b$  ( $q_a = q_b$ ), typical symmetric two-peak photoelectron ionization spectra are observed [see Fig. 2(a)]. We note that one should keep in mind that the ionization process through the state  $|1\rangle_a$  is not typical, since energy transfer without real transfer of electrons occurs. The greater the pumping parameter  $\Omega$  is, the larger is the distance between two peaks that form an Autler-Townes doublet already discussed in the literature about autoionization processes (see, e.g., [8] and references therein). These conclusions can be drawn from the positions of eight frequencies  $E_r$  in the complex plane  $E$  discussed above. Their real parts are plotted in Fig. 3(a) as a function of the pumping parameter  $\Omega$ . They create pairs with equal imaginary parts and mutual frequency difference equal to the Rabi frequency  $\delta\xi$ . Values of the imaginary parts of frequencies  $E_r$  indicate

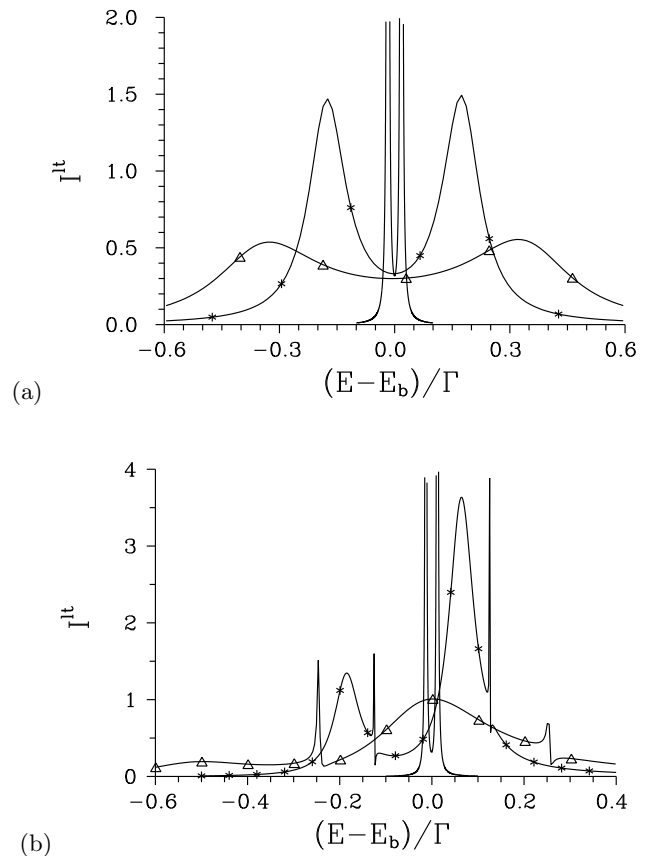


FIG. 2. Long-time photoelectron ionization spectra  $I^{\text{lt}}$  for (a)  $q_a = q_b = 100$  and (b)  $q_a = q_b = 1$  for different values of pumping parameter  $\Omega$ :  $\Omega = 0.1$  (solid curve),  $\Omega = 1$  (solid curve with \*), and  $\Omega = 2$  (solid curve with  $\Delta$ );  $\gamma_a = \gamma_b = 1$ ,  $E_a = E_b = E_L = 1$ ,  $J_{ab} = 0$ ;  $q_a = \mu_a/(\pi\mu J^*)$ ,  $\gamma_a = \pi|J|^2$ ,  $q_b = \mu_b/(\pi\mu V^*)$ ,  $\gamma_b = \pi|V|^2$ ,  $\Omega = \sqrt{4\pi\Gamma}(Q + i)\mu\alpha_L$ ,  $\Gamma = \gamma_a + \gamma_b$ ,  $Q = (\gamma_a q_a + \gamma_b q_b)/\Gamma$ . Spectra are normalized such that  $\int dE I^{\text{lt}}(E) = 1$ .

that only two pairs considerably participate in forming the long-time photoelectron spectra  $I^{\text{lt}}$ . Moreover, the frequencies  $E_r$  of these two pairs nearly coincide [see Fig. 3(a)]. This explains, why the photoelectron ionization spectra  $I^{\text{lt}}$  are composed only of two peaks. We note that a two-peak structure is preserved even in the limit of weak optical pumping. The Fano-like zero at frequency  $E = E_L$  can even be revealed for  $\Omega \rightarrow 0$ , see Sec. IV later. This distinguishes spectral profiles of the autoionization system compared to the Fano model [see Fig. 2(a) in [19]] having one central peak for weak optical pumping. Similarly as in the Fano model, the peaks broaden with the increasing pumping parameter  $\Omega$ .

If the strength of direct ionization path is comparable with those of two indirect ionization paths, the structure of long-time photoelectron ionization spectra is much richer [see Fig. 2(b)]. We can identify two sharp nearly symmetrically positioned peaks in graphs in Fig. 2(b), with the mutual distance roughly given by the Rabi frequency  $\delta\xi$ . Contrary to two symmetrically positioned

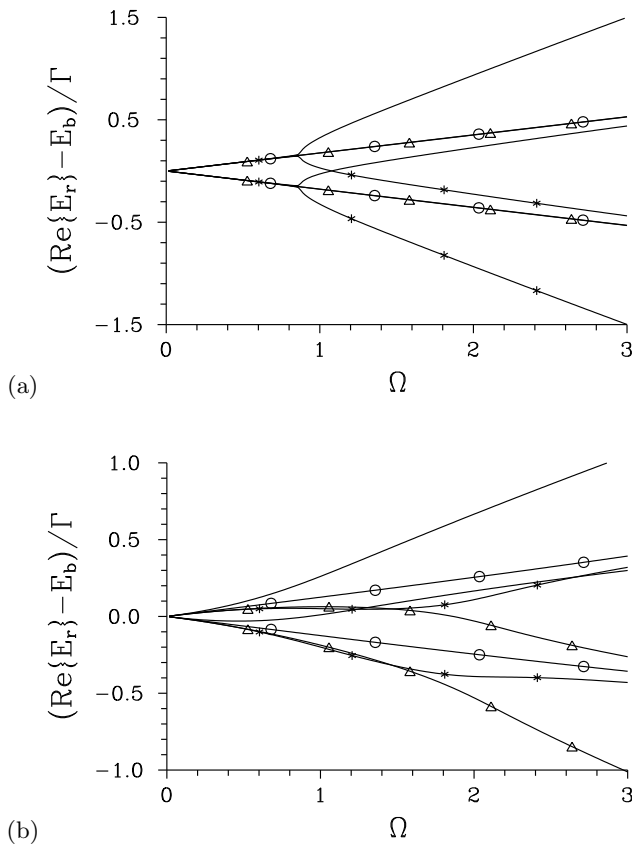


FIG. 3. Real parts of eight complex frequencies  $E_r$ ,  $E_r = \Lambda_{Me,j} + \xi_k$  for  $j = 1, \dots, 4$  and  $k = 1, 2$ , indicating the positions of poles in spectra  $I^{\text{lt}}$  for (a)  $q_a = q_b = 100$  and (b)  $q_a = q_b = 1$  as they depend on pumping parameter  $\Omega$ . Roots are divided into four pairs (plotted with different styles of curves) with equal imaginary parts and mutual frequency difference  $\delta\xi$ . Two pairs (solid curves with  $\triangle$  and  $\circ$ ) have small imaginary parts and are thus visible in the spectra  $I^{\text{lt}}$  shown in Fig. 2. The values of other parameters are given in caption to Fig. 2.

peaks observed for large values of  $q_a, q_b$  in Fig. 2(a), the widths of these peaks practically do not depend on the pumping parameter  $\Omega$ . Two additional much broader peaks have been observed in the ionization spectra in Fig. 2(b) for larger values of pumping parameter  $\Omega$ . The first peak can be found in the area around  $E_L$ , the second one occurs roughly one Rabi frequency  $\delta\xi$  on the left-hand side of the first peak. If the pumping parameter  $\Omega$  increases, widths of both peaks and the distance between the peaks constituting the Autler-Townes doublet increases. Moreover, the analysis of behavior of eight complex frequencies  $E_r$  has shown that only two frequency pairs are located near the real axis of complex frequency  $E$  and thus build the spectrum  $I^{\text{lt}}$  [see Fig. 3(b)]. This explains why the peaks are mutually shifted roughly by one Rabi frequency. We note that the behavior of the second two peaks resembles that found for the two peaks in the long-time photoelectron spectrum of the ionization system interacting with a neighbor in

[19] [compare Fig. 3(b) in [19]].

If indirect ionization including atom  $a$  prevails over the two remaining ionization channels, the long-time photoelectron ionization spectra are composed of two symmetrically positioned peaks. Moreover, the probability to ionize the state with the frequency  $E_a$  is practically zero [see Fig. 4(a)]. The greater the pumping parameter  $\Omega$  is, the larger is the distance between two peaks and the peaks are broader. This behavior is qualitatively similar to that found for two side-peaks in the spectra of the ionization system interacting with a neighbor investigated in [19] [compare Fig. 2(b) in [19]]. However, states with frequencies in the middle of the spectrum are only weakly occupied due to the interference with the additional ionization path coming through the autoionizing state  $|1\rangle_b$ .

When the autoionization exploiting state  $|1\rangle_b$  is dominant, the Autler-Townes splitting of the photoelectron ionization spectrum [22] naturally occurs, as documented in Fig. 4(b). Even a weak indirect ionization based on the presence of neighbor atom  $a$  is sufficient to split the ionization peak typical of smaller values of the pumping parameter  $\Omega$  into two symmetrically positioned side-peaks. Symmetric two-peak photoelectron ionization spectra are thus observed independently of the value of pumping parameter  $\Omega$ . The greater the pumping parameter  $\Omega$  is, the more distant and broader are the peaks.

In molecular condensates, the dipole-dipole interaction between the neighbor molecules has typical energies 1 - 10 meV, whereas energies in eV characterize the Coulomb configuration interaction. The ratio  $\gamma_a/\gamma_b$  thus equals  $10^{-4} - 10^{-6}$  in this case. As the dipole-dipole interaction is weak ( $\gamma_a \ll 1$ ), we are in the regime of  $q_a \gg 1$  assuming comparable values of the dipole moments  $\mu_a$  and  $\mu$ . The role of the state  $|1\rangle_a$  in forming the photoelectron ionization spectra is important provided that the optical pumping dipole and dipole-dipole interactions have comparable strengths. This occurs only for weaker optical pumping. The needed pumping amplitudes  $\alpha_L$  are thus by two or three orders of magnitude lower compared to those used in typical ionization experiments. An example of the dependence of the long-time photoelectron ionization spectra on the pumping parameter  $\Omega$  is shown in Fig. 5. We can see in Fig. 5(a) that the presence of molecule  $a$  leads to splitting of the spectral profile into two narrow peaks for smaller values of the pumping parameter  $\Omega$ . Widths of these peaks broaden, their mutual distance increases and their central frequencies shift towards the lower frequencies as the values of pumping parameter  $\Omega$  increase. However, the peaks are gradually absorbed into an asymmetric spectral profile found for larger values of pumping parameter  $\Omega$  [see Fig. 5(b)] and being typical for the Fano model with one autoionization level at molecule  $b$ . The role of molecule  $a$  in the formation of ionization spectra is thus negligible for sufficiently large values of the pumping parameter  $\Omega$ . On the other hand, the interaction with molecule  $a$  substantially modifies spectral profiles for smaller values of pumping parameter  $\Omega$ , as the comparison of curves in Fig. 5 and

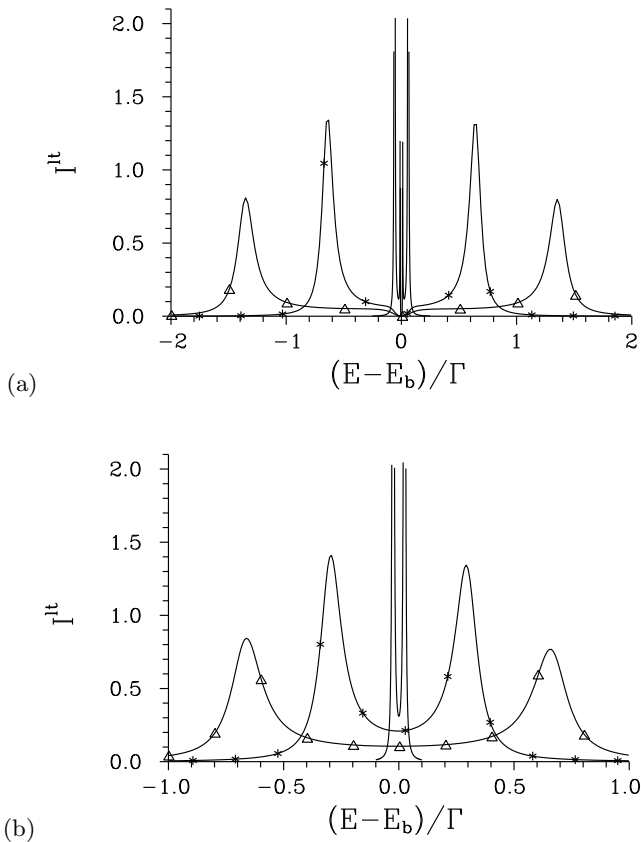


FIG. 4. Long-time photoelectron ionization spectra  $I^{lt}$  for (a)  $q_a = 100$ ,  $q_b = 1$  and (b)  $q_a = 1$ ,  $q_b = 100$  for different values of pumping parameter  $\Omega$ :  $\Omega = 0.1$  (solid curve),  $\Omega = 1$  (solid curve with \*), and  $\Omega = 2$  (solid curve with  $\Delta$ );  $\gamma_a = \gamma_b = 1$ ,  $E_a = E_b = E_L = 1$ ,  $J_{ab} = 0$ .

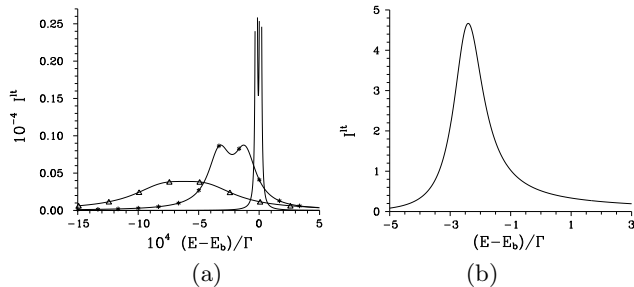


FIG. 5. Long-time photoelectron ionization spectra  $I^{lt}$  for (a)  $\Omega = 0.5 \times 10^{-2}$  (solid curve),  $\Omega = 3 \times 10^{-2}$  (solid curve with \*),  $\Omega = 5 \times 10^{-2}$  (solid curve with  $\Delta$ ) and (b)  $\Omega = 1$ ;  $q_a = 100$ ,  $\gamma_a = 1 \times 10^{-4}$ ,  $q_b = \gamma_b = 1$ ,  $E_a = E_b = E_L = 1$ ,  $J_{ab} = 0$ .

those of Fig. 3(a) in [19] clearly reveals.

Ionization spectra discussed up to now characterize the stationary long-time limit. On using the formulas written in Sec. II, temporal aspects of forming the photoelectron ionization spectra can also be addressed. As the time  $t$  increases, the initially flat photoelectron ionization spectrum is gradually ‘focused’ into its long-time shape. Naturally, the creation of sharper features in the long-time

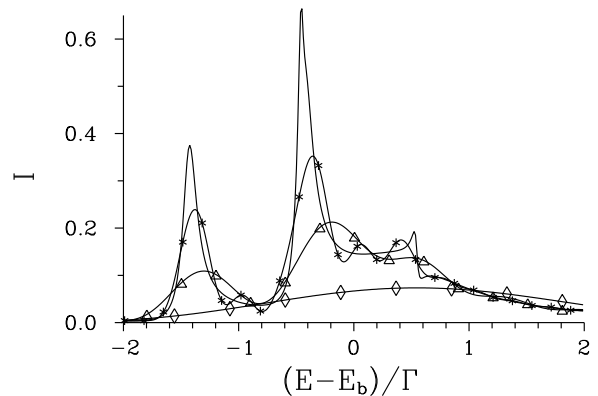


FIG. 6. Photoelectron ionization spectra  $I$  at different times  $t$  [ $I(t) = I_0(t) + I_1(t)$ ]:  $t = 1$  (solid curve with  $\diamond$ ),  $t = 5$  (solid curve with  $\Delta$ ),  $t = 10$  (solid curve with \*), and  $t \rightarrow \infty$  (solid curve). Spectrum  $I$  is determined as  $I(E, t) = |d_0(E, t)|^2 + |d_1(E, t)|^2$ ;  $q_a = q_b = \gamma_a = \gamma_b = 1$ ,  $E_a = E_b = E_L = 1$ ,  $J_{ab} = 0$ ,  $\Omega = 4$ .

spectrum requires longer times, as illustrated in Fig. 6.

#### IV. FANO AND FANO-LIKE ZEROS IN LONG-TIME PHOTOELECTRON IONIZATION SPECTRA

The Fano (Fano-like) and dynamical zeros belong to the most important features of the long-time photoelectron ionization spectra. The form of these spectra built from up to eight Lorentzian curves [see Eqs. (12), (13), and (16)] allows to draw general conclusions about the number of Fano and dynamical zeros (see Appendix B). It also allows to develop a numerical method for finding frequencies of these zeros. According to this analysis, no more than three Fano zeros can exist.

Our investigations have revealed only one Fano zero (present for arbitrarily strong pumping) under specific conditions. In the limit of weak optical pumping, two Fano-like zeros have been identified.

As for the Fano zero, its frequency  $E_F$  as well as conditions for its observation can be revealed using a suitable canonical transformation [23]. From the physical point of view, this Fano zero may occur only provided that completely destructive interference between two ionization paths at the atom  $b$  occurs as discovered in [1]. In our model, we have two additional ionization paths containing the energy transfer from the excited state  $|1\rangle_a$  of the atom  $a$ . In more detail, the first path contains direct energy transfer ( $J$ ) into the state  $|E_F\rangle$ , whereas the second additional path includes energy transfer between the states  $|1\rangle_a$  and  $|1\rangle_b$  ( $J_{ab}$ ) and the Coulomb configurational interaction ( $V$ ). These two additional ionization paths can also cancel each other under suitable conditions. A detailed analysis [23] has shown that the state  $|E_F\rangle$  in the continuum is completely decoupled from both

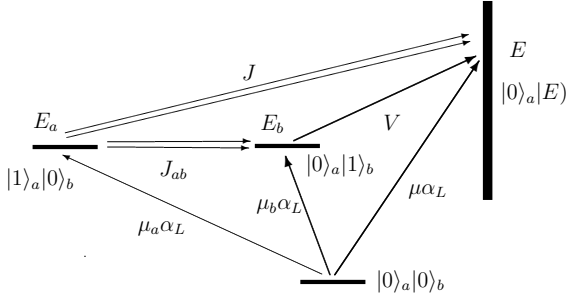


FIG. 7. Scheme of the autoionization system  $b$  interacting with the two-level atom  $a$  valid for negligible probabilities of the states with two excited or ionized electrons. The state  $|0\rangle_a|0\rangle_b$  is the ground state, the state  $|0\rangle_a|1\rangle_b$  ( $|1\rangle_a|0\rangle_b$ ) contains an excited electron at the atom  $b$  ( $a$ ), and the state  $|E\rangle|0\rangle_a$  involves an ionized electron at the atom  $b$ .

the states  $|0\rangle_b$  and  $|1\rangle_a$  only provided that [23]

$$\mu_b/\mu = J_{ab}/J. \quad (21)$$

The frequency  $E_F$  of the observed Fano zero is then given as  $E_F = E_b - \gamma_b q_b$ .

Two Fano-like zeros can be revealed in the limit of weak optical pumping, i.e., when  $\mu_a\alpha_L$ ,  $\mu_b\alpha_L$ ,  $\mu\alpha_L$  are much lower than  $V$ ,  $J$ . In this limit, the probability of having the states  $|1\rangle_a|1\rangle_b$  and  $|1\rangle_a|E\rangle$  describing two excited or ionized electrons is negligibly small compared to the other probabilities. A simplified scheme of states as shown in Fig. 7 can then be considered. This simplified model is suitable for the application of a canonical transformation [1] that gives two Fano-like zeros. This transformation 'incorporates' the states  $|0\rangle_a|1\rangle_b$  and  $|1\rangle_a|0\rangle_b$  into the states  $|E\rangle$  of the continuum.

In this simplified scheme, we consider the Hamiltonian  $\hat{H}_{ab}^{\text{oneexc}}$  that quantifies the energy of states with one excited or ionized electron:

$$\begin{aligned} \hat{H}_{ab}^{\text{oneexc}} &= E_a|1\rangle_{aa}\langle 1| + E_b|1\rangle_{bb}\langle 1| + \int dE|E\rangle\langle E| \\ &+ [J_{ab}|1\rangle_{bb}\langle 0| + \text{H.c.}] \\ &+ \int dE [J|E\rangle_b\langle 0| + \text{H.c.}] \\ &+ \int dE [V|E\rangle_b\langle 1| + \text{H.c.}]. \end{aligned} \quad (22)$$

We need to find eigenstates of the Hamiltonian  $\hat{H}_{ab}^{\text{oneexc}}$  and the corresponding dipole moments for the transitions from the ground state  $|0\rangle_a|0\rangle_b$  into the states arising from the diagonalization. We note that the spectral long-time behavior of the system with the Hamiltonian  $\hat{H}_{ab}^{\text{oneexc}}$  written in Eq. (22) has been analyzed in [24] from the point of view of dc-field coupling of two autoionizing levels.

The eigenstates  $|E\rangle$  of the Hamiltonian  $\hat{H}_{ab}^{\text{oneexc}}$  can be expressed as a linear superposition of the states  $|1\rangle_a|0\rangle_b$ ,

$|0\rangle_a|1\rangle_b$ , and  $|0\rangle_a|E\rangle$ :

$$\begin{aligned} |E\rangle &= a(E)|1\rangle_a|0\rangle_b + b(E)|1\rangle_b|0\rangle_a \\ &+ \int dE' \beta(E, E')|E'\rangle|0\rangle_a, \end{aligned} \quad (23)$$

where  $a(E)$ ,  $b(E)$ , and  $\beta(E, E')$  are the coefficients of the superposition. They obey the following system of linear algebraic equations stemming from the stationary Schrödinger equation:

$$\begin{aligned} E_a a(E) + J_{ab}^* b(E) \\ + \int dE' J^*(E') \beta(E, E') &= E a(E), \\ J_{ab} a(E) + E_b b(E) \\ + \int dE' V^*(E') \beta(E, E') &= E b(E), \\ J(E') a(E) + V(E') b(E) \\ + E' \beta(E, E') &= E \beta(E, E'). \end{aligned} \quad (24)$$

The third equation in (24) can be solved in the following form:

$$\begin{aligned} \beta(E, E') &= \frac{V(E') b(E) + J(E') a(E)}{E - E' + i\varepsilon} \\ &+ F(E) \delta(E - E'), \end{aligned} \quad (25)$$

where  $\varepsilon > 0$  ( $\varepsilon \rightarrow 0$  is assumed) and  $\delta$  means the Dirac  $\delta$ -function. The coefficient  $F(E)$  is determined from the normalization of state  $|E\rangle$ . The substitution of the solution in Eq. (25) into the first two equations in (24) gives the set of coupled equations for the coefficients  $a(E)$  and  $b(E)$ :

$$\begin{aligned} \begin{bmatrix} \tilde{E}_a - i\gamma_a - E & \tilde{J}_{ab}^* - i\pi J^*(E)V(E) \\ \tilde{J}_{ab} - i\pi J(E)V^*(E) & \tilde{E}_b - i\gamma_b - E \end{bmatrix} \\ \times \begin{bmatrix} a(E) \\ b(E) \end{bmatrix} = - \begin{bmatrix} J^*(E)F(E) \\ V^*(E)F(E) \end{bmatrix}. \end{aligned} \quad (26)$$

The damping constants  $\gamma_a$  and  $\gamma_b$  are given as  $\gamma_a = \pi|J(E_0)|^2$  and  $\gamma_b = \pi|V(E_0)|^2$  and the frequency  $E_0$  lies in the center of ionization spectrum. The renormalized frequencies  $\tilde{E}_a$  and  $\tilde{E}_b$  and the coupling constant  $\tilde{J}_{ab}$  are determined along the expressions:

$$\begin{aligned} \tilde{E}_a(E) &= E_a + \mathcal{P} \int dE' \frac{|J(E')|^2}{E - E'}, \\ \tilde{E}_b(E) &= E_b + \mathcal{P} \int dE' \frac{|V(E')|^2}{E - E'}, \\ \tilde{J}_{ab}(E) &= J_{ab} + \mathcal{P} \int dE' \frac{J(E')V^*(E')}{E - E'}, \end{aligned} \quad (27)$$

$\mathcal{P}$  denotes the principal value. The solution of two linear algebraic equations (26) can be found, e.g., by finding the inverse matrix of the system. The normalization condition  $|a(E)|^2 + |b(E)|^2 + \int dE' |\beta(E, E')|^2 = 1$  is fulfilled provided that we choose  $F(E) = 1$ . The coefficients

$a(E)$ ,  $b(E)$ , and  $\beta(E, E')$  can then be derived in their final form:

$$\begin{aligned} a(E) &= \frac{(E - \tilde{E}_b)J^*(E) + \tilde{J}_{ab}^*V^*(E)}{\mathcal{D}(E)}, \\ b(E) &= \frac{(E - \tilde{E}_a)V^*(E) + \tilde{J}_{ab}J^*(E)}{\mathcal{D}(E)}, \\ \beta(E, E') &= \frac{V(E')b(E) + J(E')a(E)}{E - E' + i\varepsilon} \\ &\quad + \delta(E - E'). \end{aligned} \quad (28)$$

The symbol  $\mathcal{D}(E)$  in Eq. (28) stands for the determinant of the matrix in Eq. (26) that is given as:

$$\begin{aligned} \mathcal{D}(E) &= (E - \tilde{E}_a)(E - \tilde{E}_b) + i\gamma_a(E - \tilde{E}_b) \\ &\quad + i\gamma_b(E - \tilde{E}_a) - |\tilde{J}_{ab}|^2 + 2i\text{Re}\{t(E)\}. \end{aligned} \quad (29)$$

In Eq. (29),  $t(E) = \pi\tilde{J}_{ab}^*J(E)V^*(E)$ . The function  $t(E)$  is nonzero only if the energy transfer between the excited states  $|1\rangle_a$  and  $|1\rangle_b$  occurs.

The optical-field interaction between the ground state  $|0\rangle_a|0\rangle_b$  and the states with one excited or ionized electron as described by the Hamiltonian  $\hat{H}_{ab}^{\text{oneexc}}$  is governed by the Hamiltonian  $\hat{H}_{ab}^{\text{opt}}$ :

$$\begin{aligned} \hat{H}_{ab}^{\text{opt}} &= [\mu_a\alpha_L \exp(-iE_L t)|1\rangle_{aa}\langle 0|0\rangle_{bb}\langle 0| + \text{H.c.}] \\ &\quad + [\mu_b\alpha_L \exp(-iE_L t)|1\rangle_{bb}\langle 0|0\rangle_{aa}\langle 0| + \text{H.c.}] \\ &\quad + \int dE [\mu\alpha_L \exp(-iE_L t)|E\rangle_b\langle 0|0\rangle_{aa}\langle 0| + \text{H.c.}]. \end{aligned} \quad (30)$$

The Hamiltonian  $\hat{H}_{ab}^{\text{opt}}$  transformed into the basis  $|0\rangle_a|0\rangle_b$  and  $|E\rangle$  reads:

$$\hat{H}_{ab}^{\text{opt}} = \int dE [\bar{\mu}(E)\alpha_L \exp(-iE_L t)|E\rangle_a\langle 0|_b\langle 0| + \text{H.c.}]. \quad (31)$$

The dipole moment  $\bar{\mu}$  in the transformed basis is given by the formula

$$\bar{\mu}(E) = \mu_a a^*(E) + \mu_b b^*(E) + \int dE' \mu(E')\beta^*(E, E'). \quad (32)$$

This formula can be recast into the following form:

$$\begin{aligned} \bar{\mu}(E) &= \left[ 1 + \frac{(q_a + i)[\gamma_a(E - \tilde{E}_b) + t^*]}{\mathcal{D}^*(E)} \right. \\ &\quad \left. + \frac{(q_b + i)[\gamma_b(E - \tilde{E}_a) + t]}{\mathcal{D}^*(E)} \right] \mu(E). \end{aligned} \quad (33)$$

We remind that the parameters  $q_a$  and  $q_b$  are defined in the caption to Fig. 2.

The frequencies  $E_F$  giving the positions of Fano-like zeros can be easily identified using the condition  $\bar{\mu}(E_F) = 0$  in Eq. (33). This leads to the quadratic equation:

$$\begin{aligned} [E - \tilde{E}_b]^2 &+ [-\tilde{E}_a + \tilde{E}_b + q_a\gamma_a + q_b\gamma_b][E - \tilde{E}_b] \\ &+ [q_a t^* + q_b(t - \gamma_b\tilde{E}_a + \gamma_b\tilde{E}_b) - |\tilde{J}_{ab}|^2] = 0. \end{aligned} \quad (34)$$

The solution of quadratic equation (34) reveals the frequencies  $E_F$  of at most two Fano zeros:

$$[E_F]_{1,2} = \frac{\tilde{E}_a + \tilde{E}_b - q_a\gamma_a - q_b\gamma_b}{2} \pm \frac{\sqrt{D}}{2}. \quad (35)$$

They occur for a non-negative discriminant  $D$ ,

$$\begin{aligned} D &= (\tilde{E}_a - \tilde{E}_b)^2 + (q_a\gamma_a + q_b\gamma_b)^2 - 2(\tilde{E}_a - \tilde{E}_b) \\ &\quad \times (q_a\gamma_a - q_b\gamma_b) + 4|\tilde{J}_{ab}|^2 - 4q_a t^* - 4q_b t. \end{aligned} \quad (36)$$

We note that the frequencies  $E_F$  of two Fano zeros written in Eq. (36) coincide with those revealed in [7] for a double Fano system provided that  $\tilde{J}_{ab} = 0$ .

## V. DYNAMICAL ZEROS IN LONG-TIME PHOTOELECTRON IONIZATION SPECTRA

The analysis contained in Appendix B reveals that up to 15 dynamical zeros can exist. Their frequencies  $E_D$  can be determined along the recipe described in Appendix B. We should note that frequencies  $E_D$  of two of the dynamical zeros coincide with the frequencies  $E_F$  of the Fano-like zeros discussed in Sec. IV in the limit of weak optical pumping. If we plot the normalized frequencies  $(E_D - E_b)/\Gamma$  of dynamical zeros as functions of the pumping parameter  $\Omega$ , we arrive at graphs similar in shape to those appearing in the model of ionization system interacting with a neighbor (see Fig. 6 in [19]). Graphs obtained for the analyzed model are in general more complex. However, creation and annihilation of dynamical zeros in pairs represents their most typical feature. As an example, the graphs corresponding to the values of parameters defined in the caption to Fig. 2 are shown in Fig. 8. They demonstrate the 'creation' and 'annihilation' of dynamical zeros in pairs. However, dynamical zeros can emerge even in greater numbers. This is documented in Fig. 9 where even five dynamical zeros occur with frequency  $E_D = E_b$  for  $\Omega = 0$  for values of parameters typical for molecular condensates. Similarly as in the long-time photoelectron ionization spectra of the ionization system interacting with a neighbor [19], splitting of the normalized frequencies  $(E_D - E_b)/\Gamma$  appropriate to the spectra  $I_0^{\text{lt}}$  and  $I_1^{\text{lt}}$  is observed for non-resonant pumping of the two-level atom  $a$  ( $E_a \neq E_L$ ). The symmetry  $\Omega \leftrightarrow -\Omega$  mentioned in [19] is also preserved in the analyzed autoionization system.

## VI. CONCLUSIONS

The long-time photoelectron ionization spectra of an autoionization system interacting with a neighbor two-level atom have been investigated in several distinct regimes. They typically consist of several peaks with central positions and spectral widths depending on the pumping strength. As a consequence of interference of



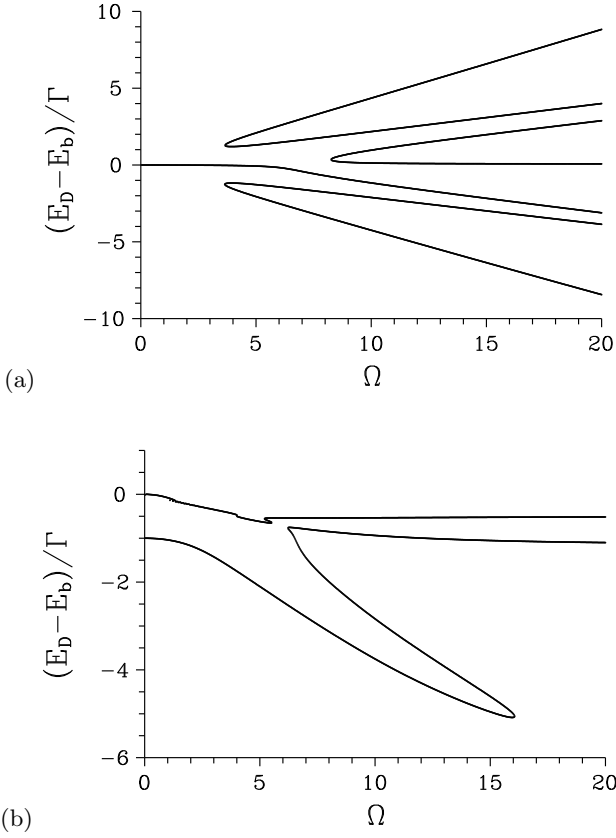


FIG. 8. Normalized frequencies  $(E_D - E_b)/\Gamma$  of dynamical zeros as they depend on pumping parameter  $\Omega$  for resonant pumping of atom  $a$ : (a)  $q_a = q_b = 100$ , (b)  $q_a = q_b = 1$ ;  $\gamma_a = \gamma_b = 1$ ,  $E_a = E_b = E_L = 1$ ,  $J_{ab} = 0$ .

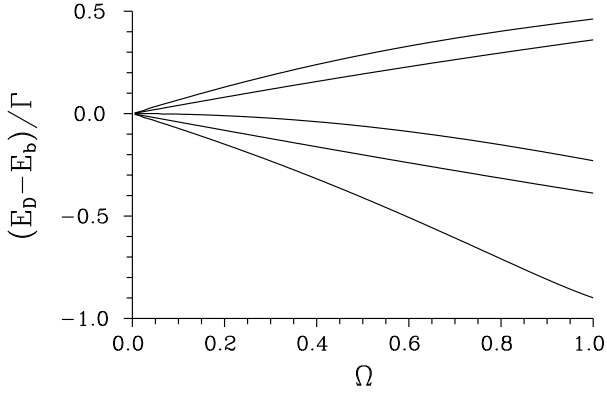


FIG. 9. Normalized frequencies  $(E_D - E_b)/\Gamma$  of dynamical zeros as they depend on pumping parameter  $\Omega$  for resonant pumping of atom  $a$ : values of parameters are written in the caption to Fig. 5.

several ionization paths, zeros in the long-time photoelectron ionization spectral profiles occur. Whereas only one genuine Fano zero has been found under special conditions, two Fano-like zeros observed only for weak optical pumping have been identified for a general system constructing a suitable canonical transformation. The

long-time photoelectron ionization spectra conditioned by the state of the neighbor two-level atom exhibit permanent Rabi oscillations. Spectral dynamical zeros observed once in the Rabi period have been revealed in these spectra. The frequencies of these dynamical zeros depending on the strength of optical pumping as well as the projected state of the neighbor two-level atom have been analyzed.

## ACKNOWLEDGMENTS

Support by the projects 1M06002, COST OC 09026, and Operational Program Research and Development for Innovations - European Social Fund (project CZ.1.05/2.1.00/03.0058) of the Ministry of Education of the Czech Republic as well as the project IAA100100713 of GA AV ČR is acknowledged.

## Appendix A: Determination of poles of the Lorentzian curves giving photoelectron spectra

The complex frequencies  $E_r$  giving poles of the Lorentzian curves composing photoelectron ionization spectra are determined as a sum of eigenvalues  $\Lambda_{M^e, j}$  of the matrix  $\mathbf{M}^e$  ( $j = 1, \dots, 4$ ) and frequencies  $\xi_k$  ( $k = 1, 2$ ) giving the Rabi oscillations of two-level atom  $a$ ;  $E_r = \Lambda_{M^e, j} + \xi_k$ . Whereas the frequencies  $\xi_k$  are written in Eq. (11), the eigenvalues  $\Lambda_{M^e, j}$  can be derived from roots of the fourth-order polynomial written in the shifted frequency  $\tilde{\Lambda}_{M^e}$ ;  $\Lambda_{M^e} = \tilde{\Lambda}_{M^e} - i\pi|\mu\alpha_L|^2$ :

$$[\tilde{\Lambda}_{M^e}]^4 + \alpha_3[\tilde{\Lambda}_{M^e}]^3 + \alpha_2[\tilde{\Lambda}_{M^e}]^2 + \alpha_1\tilde{\Lambda}_{M^e} + \alpha_0 = 0. \quad (\text{A1})$$

The coefficients  $\alpha_j$  introduced in Eq. (A1) can be derived from the elements of matrix  $\mathbf{M}^e$ :

$$\begin{aligned} \alpha_0 &= (\Delta E_a + \mathcal{E}_b) [-\mathcal{E}_b M_a M_a^c + (-\Delta E_a + i\gamma_a) M_b M_b^c \\ &\quad + (M_a M_b^c j_{ab} + M_a^c M_b j_{ab}^c)] |\alpha_L|^2 + [M_a M_a^c |\mu_a|^2 \\ &\quad + M_b^2 M_b^c - (M_a \mu_a^* + M_a^c \mu_a) M_b M_b^c] |\alpha_L|^4, \\ \alpha_1 &= (-\Delta E_a + i\gamma_a)(\Delta E_a + \mathcal{E}_b) \mathcal{E}_b + [(\Delta E_a - i\gamma_a) |\mu_a|^2 \\ &\quad + (\Delta E_a + 2\mathcal{E}_b) M_a M_a^c + (2\Delta E_a - i\gamma_a + 2\mathcal{E}_b) \\ &\quad \times M_b M_b^c] |\alpha_L|^2 + (\Delta E_a + \mathcal{E}_b) j_{ab} j_{ab}^c \\ &\quad - [(\mu_a + M_a) M_b^c j_{ab} + (\mu_a^* + M_a^c) M_b j_{ab}^c] |\alpha_L|^2, \\ \alpha_2 &= \Delta E_a (\Delta E_a - i\gamma_a) + (3\Delta E_a - 2i\gamma_a) \mathcal{E}_b + \mathcal{E}_b^2 \\ &\quad - [M_a M_a^c + |\mu_a|^2 + 2M_b M_b^c] |\alpha_L|^2 - j_{ab} j_{ab}^c, \\ \alpha_3 &= -2\Delta E_a - 2\mathcal{E}_b + i\gamma_a. \end{aligned} \quad (\text{A2})$$

In Eq. (A2),  $\mathcal{E}_b = \Delta E_b - i\gamma_b + i\pi|\mu\alpha_L|^2$ ,  $M_a = \mu_a - i\pi\mu J^*$ ,  $M_a^c = \mu_a^* - i\pi\mu^* J$ ,  $M_b = \mu_b - i\pi\mu V^*$ ,  $M_b^c = \mu_b^* - i\pi\mu^* V$ ,  $j_{ab} = J_{ab} - i\pi J V^*$ , and  $j_{ab}^c = J_{ab}^* - i\pi J^* V$ . Roots of the polynomial in Eq. (A1) can be found analytically, in principle, which might be useful in special cases.

## Appendix B: Determination of Fano and dynamical zeros

The specific form of the long-time solution for the photoelectron spectra written in Eqs. (12), (13), and (16) allows to reformulate the condition in Eq. (19) for the frequencies  $E_F$  of Fano zeros. They can be found as a common solution of the following four equations:

$$\sum_{j=1}^4 \frac{A_j^{kl}}{E - \Lambda_{M^e, j} - \xi_l} = 0; \quad k = 0, 1, \quad l = 1, 2. \quad (\text{B1})$$

The coefficients  $A_j^{kl}$  can be derived from the solution in Eq. (13) as follows:

$$A_j^{kl} = [\mathbf{K}_1 \mathbf{B}^{e\dagger} \mathbf{P}^e]_{kj} [\mathbf{P}^{e-1} \mathbf{c}(0)]_j. \quad (\text{B2})$$

Equations in (B2) can be recast into the form of the third-order polynomials  $p_{kl}(E)$ :

$$p_{kl}(E) = \sum_{j=0}^3 \alpha_j^{kl} E^j = 0 \quad (\text{B3})$$

with the coefficients defined as:

$$\alpha_0^{kl} = - \sum_{j=1}^4 A_j^{kl} \prod_{m=1, m \neq j}^4 (\Lambda_{M^e, m} + \xi_l),$$

$$\alpha_1^{kl} = \sum_{j=1}^4 A_j^{kl} \sum_{m=1, m \neq j}^4 (\Lambda_{M^e, m} + \xi_l)$$

$$\times \sum_{n=1, n \neq j, m}^4 (\Lambda_{M^e, n} + \xi_l),$$

$$\alpha_2^{kl} = - \sum_{j=1}^4 A_j^{kl} \sum_{m=1, m \neq j}^4 (\Lambda_{M^e, m} + \xi_l),$$

$$\alpha_3^{kl} = \sum_{j=1}^4 A_j^{kl}. \quad (\text{B4})$$

A Fano zero is identified only provided that its frequency  $E_F$  is found simultaneously among three roots of the polynomials  $p_{kl}$  for all  $k = 0, 1$  and  $l = 1, 2$ . Moreover, the corresponding root has to be real. In general, no more than three Fano zeros can be found.

The third-order polynomials  $p_{kl}$  introduced in Eq. (B3) are also useful in expressing the conditions  $|d_k^{\xi_1}(E, t)| = |d_k^{\xi_2}(E, t)|$  [equivalent to those written in Eq. (20)] for the occurrence of dynamical zeros in the spectra  $I_k^{\text{lt}}$ ,  $k = 0, 1$ :

$$|p_{k1}(E)| \prod_{j=1}^4 |E - \Lambda_{M^e, j} - \xi_2|$$

$$= |p_{k2}(E)| \prod_{j=1}^4 |E - \Lambda_{M^e, j} - \xi_1|, \quad k = 0, 1. \quad (\text{B5})$$

Equation (B5) represents a fifteenth-order polynomial which can have complex coefficients. If a root of this polynomial is real, it gives the frequency  $E_D$  of a dynamical zero. In principle, up to 15 dynamical zeros might exist.

- 
- [1] U. Fano, Phys. Rev. **124**, 1866 (1961).  
[2] K. Rzażewski and J. H. Eberly, Phys. Rev. Lett. **47**, 408 (1981).  
[3] M. Lewenstein, J. W. Haus, and K. Rzażewski, Phys. Rev. Lett. **50**, 417 (1983).  
[4] J. W. Haus, M. Lewenstein, and K. Rzażewski, Phys. Rev. A **28**, 2269 (1983).  
[5] G. S. Agarwal, S. L. Haan, and J. Cooper, Phys. Rev. A **29**, 2552 (1984).  
[6] K. Rzażewski and J. H. Eberly, Phys. Rev. A **27**, 2026 (1983).  
[7] W. Leoński, R. Tanaś, and S. Kielich, J. Opt. Soc. Am. B **4**, 72 (1987).  
[8] W. Leoński and R. Tanaś, J. Phys. B: At. Mol. Opt. Phys. **21**, 2835 (1988).  
[9] P. Lambropoulos and P. Zoller, Phys. Rev. A **24**, 379 (1981).  
[10] L. Journel, B. Rouvellou, D. Cubaynes, J. M. Bizau, F. J. Willeumier, M. Richter, P. Sladeczek, K.-H. Selbman, P. Zimmerman, and H. Bergerow, J. de Physique IV **3**, 217 (1993).  
[11] E. Paspalakis, N. J. Kylstra, and P. L. Knight, Phys. Rev. A **60**, 642 (1999).  
[12] A. Raczyński, M. Rzepecka, J. Zaremba, and S. Zielińska-Kaniasty, Optics Communications **266**, 552 (2006).  
[13] M. Lewenstein and K. Rzażewski, Phys. Rev. A **61**, 022105 (2000).  
[14] W. Leoński and V. Bužek, J. Mod. Opt. **37**, 1923 (1990).  
[15] W. Leoński, J. Opt. Soc. Am. B **10**, 244 (1993).  
[16] P. Durand, I. Paidarová, and F. X. Gadéa, J. Phys. B: At. Mol. Opt. Phys. **34**, 1953 (2001).  
[17] A. E. Miroshnichenko, S. Flach, and Y. S. Kivshar, Rev. Mod. Phys. **82**, 2257 (2010).  
[18] W. Leoński, R. Tanaś, and S. Kielich, J. Phys. D: Appl. Phys. **21**, S125 (1988).  
[19] J. Peřina Jr., A. Lukš, W. Leoński, and V. Peřinová, Phys. Rev. A p. in print (2011).  
[20] E. A. Silinsh and V. Čápek, *Organic Molecular Crystals: Interaction, Localization and Transport Phenomena* (Oxford University Press/American Institute of Physics, 1994).  
[21] P. Meystre and P. Sargent III, *Elements of Quantum Optics* (Springer, Berlin, 2007).  
[22] S. H. Autler and C. H. Townes, Phys. Rev. **100**, 703 (1955).  
[23] A. Lukš, V. Peřinová, J. Peřina Jr., J. Křepelka, and W. Leoński, in *Wave and Quantum Aspects of Contemporary Optics: Proceedings of SPIE, Vol. 7746*, edited by J. Müllerová, D. Senderáková, and S. Jurecka (SPIE, Bellingham, 2010), p. 77460W.  
[24] W. Leoński and R. Tanaś, J. Opt. Soc. Am. B **8**, 6 (1991).